

Manipulation of γ -ray polarization in Compton scattering

Yu Wang,¹ Mamutjan Ababekri,¹ Feng Wan,¹ Jia-Xing Wen,² Wen-Qing Wei,¹ Zhong-Peng Li,¹ Hai-Tao Kang,¹ Bo Zhang,^{2,*} Yong-Tao Zhao,¹ Wei-Min Zhou,^{2,†} and Jian-Xing Li^{1,‡}

¹*Ministry of Education Key Laboratory for Nonequilibrium Synthesis and Modulation of Condensed Matter, Shaanxi Province Key Laboratory of Quantum Information and Quantum Optoelectronic Devices, School of Physics, Xi'an Jiaotong University, Xi'an 710049, China*

²*Key laboratory of plasma physics, Research center of laser fusion,*

China academy of engineering physics, Mianshan Rd 64#, Mianyang, Sichuan 621900, China

(Dated: July 21, 2023)

High-brilliance high-polarization γ rays based on Compton scattering are of great significance in broad areas, such as nuclear, high-energy, astro-physics, etc. However, the transfer mechanism of spin angular momentum in the transition from linear, through weakly into strongly nonlinear processes is still unclear, which severely limits the simultaneous control of brilliance and polarization of high-energy γ rays. In this work, we investigate the manipulation mechanism of high-quality polarized γ rays in Compton scattering of the ultrarelativistic electron beam colliding with an intense laser pulse. We find that the contradiction lies in the simultaneous achievement of high-brilliance and high-polarization of γ rays by increasing laser intensity, since the polarization is predominately contributed by the electron (laser photon) spin via multi-photon (single-photon) absorption channel. Moreover, we confirm that the signature of γ -ray polarization can be applied for observing the nonlinear effects (multi-photon absorption) of Compton scattering with moderate-intensity laser facilities.

Polarized γ rays are powerful probes for basic researches and applications [1–5]. For instances, polarized photons below 1 MeV enable the crystallographic probing and the biomedical imaging with femtosecond time resolution [4]. In the energy range of several MeV to tens of MeV, polarized photo-induced nuclear reactions are highly effective in studying nuclear physics, transmutation and astrophysics [6–9]. Furthermore, polarized γ rays can be readily deployed for testing the interaction between two real photons leading to the linear Breit-Wheeler (BW) electron-positron pair production [10–12] and photon-photon elastic scattering [13, 14]. For energy scales ranging from hundreds of MeV to GeV, polarized γ rays are significant for probing vacuum birefringence [15–17].

Traditionally, polarized γ -ray sources are mainly obtained via synchrotron radiation [4, 18], bremsstrahlung [19, 20], and linear Compton scattering (LCS) [21–23]. For synchrotron radiation facilities, as the energy of γ rays $\varepsilon_\gamma \propto \varepsilon_e^2/\lambda$ [24, 25], higher-energy electrons are required because of the insertion devices of undulators (wigglers) with the wavelength λ of a few centimeters, where ε_e is the electron energy. Compared with bremsstrahlung, LCS is characterized by good directionality, collimation and high polarization [26, 27]. However, the low scattering probability sets a practical limit for the maximum flux no larger than 10^{10} photons·s⁻¹ [8].

Recently, the rapidly advanced high-power laser technique [28–31] has promoted the research of high-energy high-brilliance polarized γ rays [27, 32, 33], where the interaction mechanism transitions from linear into the nonlinear regime [34–37]. At intermediate laser intensity, polarized γ rays can be generated by spin-nonpolarized (SNP) electron beams via weakly nonlinear CS (NLCS) [38–41]. Furthermore, the stronger laser field scattered with initially spin-polarized (SP)

electron beams enables the generation of more brilliant high-polarization γ rays in strongly NLCS [42]. Importantly, in the near future, experiments such as LUXE at DESY [43] and E320 at FACET-II [44] will be performed using the conventionally accelerated $\varepsilon_e \sim 10$ GeV electron beam in collision with dozens up to hundreds of TW (corresponding to the laser invariant intensity $a_0 \sim 10$) laser pulse to probe the transition from linear to strongly nonlinear QED regime. Moreover, all-optical PW up to 10 PW laser facilities have also been commissioned or will be online [45–49]. However, there is no charted transfer mechanism of spin angular momentum (SAM) in the transition from linear, through weakly into strongly nonlinear CS. Therefore, controlling the brilliance and polarization of high-energy γ rays is still a great challenge.

In this Letter, the manipulation of γ -ray polarization in CS employing the S(N)P ultrarelativistic electron beam is investigated. We find that the contradiction lies in the simultaneous achievement of high-brilliance and high-polarization of γ rays by increasing laser intensity, since the polarization is predominately contributed by the electron (laser photon) spin via multi-photon (single-photon) absorption channel (see Figs.1 and 2). And, SNP electrons in high-intensity laser pulse can also generate high-brilliance high-polarization γ photons (see Fig.3). The transfer mechanism of SAM is also valid in the generation of vortex γ photons due to the same radiation dynamics as the plane-wave γ photons [50]. Moreover, the polarization of γ photons radiated by the electrons with different initial spin states proceeds in different ways in LCS and strongly NLCS respectively, which can give a clear evidence of the nonlinear effects in CS with moderate-intensity laser facilities (see Fig.4).

When electrons scatter with a laser pulse, they may absorb single or multiple low-energy laser photons and then emit a high-energy γ photon via CS. The polarization-dependent transition rate summing over the final electron spin in a circularly

* zhangbolfr@caep.cn

† zhouwm@caep.cn

‡ jianxing@xjtu.edu.cn

polarized (CP) monochromatic field is given by [35, 51]

$$\frac{dW}{dt} = W_0 \sum_{n=1}^{\infty} \int_0^{\delta_n} d\delta [F_{1n} + h_L h_e F_{2n} + h_\gamma (h_L F_{3n} + h_e F_{4n})], \quad (1)$$

where, $W_0 = \alpha m_e^2 a_0^2 / (8\varepsilon_{\text{eff}})$, $a_0 = |e|E / (m_e \omega_L)$ is the laser invariant intensity, $\varepsilon_{\text{eff}} = \varepsilon_e + a_0^2 \omega_L / \Lambda$ the effective energy of initial electron in the laser field, $\delta = (k_L \cdot k_\gamma) / (k_L \cdot p) \approx \varepsilon_\gamma / \varepsilon_e$ the energy ratio parameter, $\delta_n = n\Lambda / (1 + a_0^2 + n\Lambda)$ the cutoff-energy fraction of emitted photon absorbing n laser photons, i.e., n -th Compton edge [35], $\Lambda = 2(k_L \cdot p) / m_e^2$ the invariant variable, p , k_L and k_γ the four-momenta of the initial electron, laser photon and emitted photon, respectively, α the fine structure constant, e and m_e the charge and rest mass of the electron, and ω_L and E the frequency and amplitude of the laser field, respectively. Relativistic units with $c = \hbar = 1$ are used throughout. F_{kn} ($k = 1, 2, 3, 4$) in Eq. (1) are detailed in [52]. h_L , h_e and h_γ are helicities of the laser, initial electron, and emitted photon, respectively. The helicity of emitted γ photon is determined by [35, 51]

$$h_\gamma = \frac{h_L F_3 + h_e F_4}{F_1 + h_L h_e F_2}, \quad (2)$$

where, $F_k = \sum_{n=1}^{\infty} F_{kn}$ ($k = 1, 2, 3, 4$, respectively). The polarization of γ photon hardly changes during the subsequent propagation [51–53].

The transfer mechanism of SAM in CS from linear to strongly nonlinear processes is illustrated in Fig.1. For $a_0 \lesssim O(0.1)$, there is a distinct edge at the end of the first harmonic followed by smaller probabilities of higher harmonics [see Figs.3(a) and .3(b)]. For instance, for $a_0 = 0.1$, $\frac{d^2 W_{\text{rad}}}{d\delta d\delta} \approx 10^{-5.31}$ at $\delta \approx 0.192$ is two orders of magnitude smaller than $\frac{d^2 W_{\text{rad}}}{d\delta d\delta} \approx 10^{-3.01}$ at $\delta = \delta_1 \approx 0.190$, and for larger δ , $\frac{d^2 W_{\text{rad}}}{d\delta d\delta}$ is smaller, where W_{rad} is the radiation probability after summing over the emitted photon helicity and averaging over the initial electron spin with $\frac{d^2 W_{\text{rad}}}{d\delta d\delta} = 2W_0 \sum_{n=1}^{\infty} F_{1n}$, and δ_1 is the first Compton edge of the emitted photon. Therefore, for $a_0 \lesssim O(0.1)$, the electron absorbs almost only one laser photon and radiates a γ photon with $\delta \leq \delta_1$, i.e., the scattering process is LCS. For $a_0 \sim O(1)$, the process of absorbing dozens of laser photons appears with $\frac{d^2 W_{\text{rad}}}{d\delta d\delta} \approx 10^{-2.99}$ of the average number of absorbed laser photons $\bar{n} = 10$ (corresponding to $\delta \approx 0.4$), termed as weakly NLCS. As a_0 increases to $O(10)$, due to $W_{\text{rad}} \propto a_0^2$, the electron will have a greater probability of absorbing thousands of laser photons to emit a higher-energy γ photon with $\frac{d^2 W_{\text{rad}}}{d\delta d\delta} \approx 10^{-1.22}$ of $\bar{n} = 1000$ (corresponding to $\delta \approx 0.55$), described as strongly NLCS. Therefore, electrons will radiate more brilliant γ rays in higher-intensity laser field. Due to $\delta_n \propto 1/a_0^2$ for a given n , the harmonic cutoffs decrease as a_0 increases, e.g., $\delta_1 \approx 0.190$ for $a_0 = 0.1$ while $\delta_1 \approx 0.0023$ for $a_0 = 10$. Besides, for a certain a_0 the gaps of harmonic cutoffs $\Delta\delta_n = \delta_n - \delta_{n-1} \propto 1/n^2$ decrease with absorbing more laser photons [see examples of four lines corresponding to the first four cutoffs $\delta_{n=1,2,3,4}$ in Fig. 1(a)]. Therefore, the harmonic structure is clearly visible in linear and weakly nonlinear CS spectra, however, which

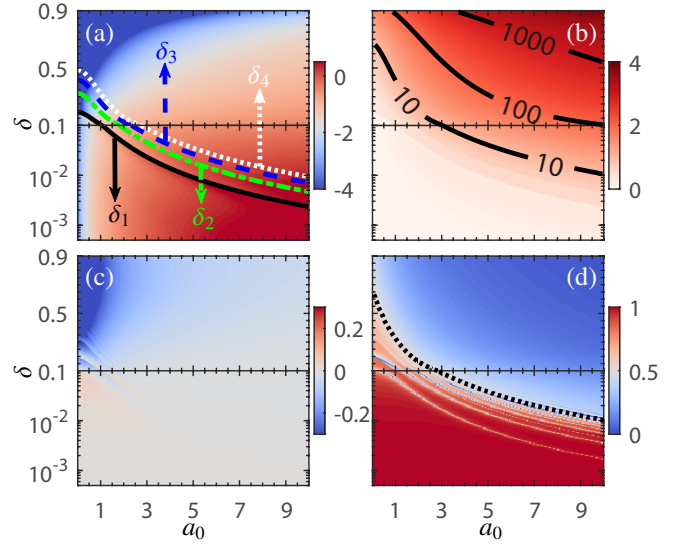


FIG 1. (a) Distribution of the total differential transition rate $\log_{10} \frac{d^2 W_{\text{rad}}}{d\delta d\delta}$ after summing over the photon helicity and averaging over the initial electron spin versus the laser invariant intensity a_0 and energy ratio parameter δ , where $\frac{d^2 W_{\text{rad}}}{d\delta d\delta} = 2W_0 \sum_{n=1}^{\infty} F_{1n}$ with $\omega_L = 1.55$ eV and $\varepsilon_e = 10$ GeV. The black-solid, green-dash-dotted, blue-dashed, and white-dotted lines indicate the first four cutoffs $\delta_{n=1,2,3,4}$, respectively. (b) Average number of absorbed laser photons $\log_{10} \bar{n}$ versus a_0 and δ . The black-solid lines indicate the contour lines of $\bar{n} = 10, 100$ and 1000 , respectively. Ratios of (c) $\frac{F_2}{F_1}$ and (d) $\frac{|F_3|}{|F_3|+F_4}$ ($F_4 > 0$) versus a_0 and δ , respectively. The black-dotted line in (d) indicates the spin contribution of the laser is equal to that of an electron to the γ photon, i.e., $\frac{|F_3|}{|F_3|+F_4} = 0.5$.

becomes smoother in strongly NLCS. Importantly, the impact of electron spin on the transition rate weakens as the laser intensity increases. For instances, for $a_0 = 0.1$, the radiation probability of the longitudinally spin-polarized (LSP) electrons (satisfying $h_L h_e = -1$) at the first edge can be increased by $\Delta W_i = (W_i^{\text{LSP}} - W_i^{\text{SNP}}) / W_i^{\text{SNP}} = -\frac{F_2}{F_1} \approx 20\%$, yet, for $a_0 = 10$, $\Delta W_i \sim 0$ [see Fig.1(c)], where W_i^{LSP} (W_i^{SNP}) is the radiation probability of LSP (SNP) electrons after summing over the emitted photon polarization in Eq.(1).

The electron spin plays an increasingly significant role in the transfer of SAM with stronger nonlinear effects. The entanglement term $\frac{F_2}{F_1}$ of the laser helicity and electron spin in the photon helicity Eq.(2) mainly operates at the end of the first few harmonics and decreases as a_0 increases. While $\frac{F_2}{F_1}$ can reach to -0.68 at $\delta = 0.7$ for $a_0 = 0.1$, it is irrelevant due to the relatively low radiation probability with $\frac{d^2 W_{\text{rad}}}{d\delta d\delta} \approx 10^{-25}$ [see Figs.1(a) and 1(c)]. Therefore, the helicity of emitted γ photon is mainly related to the independent laser helicity term F_3 and electron spin term F_4 . For emitted photons with $\delta \lesssim \delta_1$ at any a_0 , the laser helicity contribution $\frac{|F_3|}{|F_3|+F_4} \approx 1$ and correspondingly the electron spin contribution $\frac{F_4}{|F_3|+F_4} = 1 - \frac{|F_3|}{|F_3|+F_4} \approx 0$, i.e., regardless of whether the scattering process is linear or not, the average helicity of γ photons via the single-photon channel

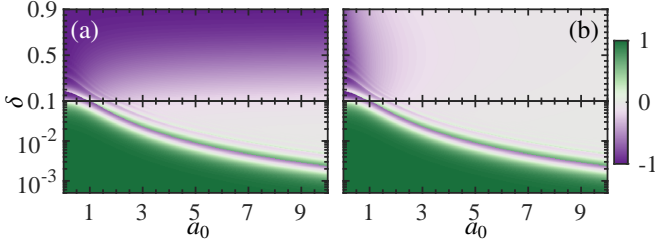


FIG 2. Average helicity \bar{h}_γ of the emitted photons versus a_0 and δ for two different models of (a) the laser helicity $h_L = 1$ and initial electron helicity $h_e = -1$, and (b) $h_L = 1$ and $h_e = 0$, respectively. The laser and electron-beam parameters are the same as those in Fig. 1.

is almost completely determined by the laser [see Fig. 1(d)]. When electrons simultaneously absorb dozens of laser photons, higher-energy γ photons are emitted, where the laser helicity contribution gradually decreases and the electron spin comes into play, i.e., the SAM transfer enters into a competitive stage of the laser and electron for controlling the γ -photon polarization [see the black-dotted line in Fig. 1(d), which almost corresponds to $\bar{n} = 10$ in Fig. 1(b)]. As the number of absorbed laser photons continues to increase, the electron spin plays a dominant role in the SAM transfer, for instance, as \bar{n} up to 1000, $\frac{|F_3|}{|F_3|+F_4} \approx 0.05$ and $\frac{F_4}{|F_3|+F_4} \approx 0.95$ at $\delta = 0.55$ for $a_0 = 10$.

The transfer mechanism of SAM points a direction for manipulating the polarization of γ rays. For LSP ($h_e = -1$) electrons scattered with the CP ($h_L = 1$) laser, in LCS ($a_0 \lesssim 0.1$), the emitted photons are almost completely radiated by the single-photon absorption channel and helicities are mainly contributed by the laser [see Fig. 2(a)]. In the low-energy parts of the first harmonic, γ photons are radiated in the forward scattering with average helicity $\bar{h}_\gamma \simeq h_L = 1$, while near the edge $\bar{h}_\gamma \simeq -h_L = -1$ via the backward scattering [54]. As a_0 increases, the interaction process transitions into the NLCS regime, due to $\delta_1 \propto 1/a_0^2$, the energy regions of $\bar{h}_\gamma \sim 1$ of radiated photons via the single-photon channel tend toward lower-energy areas with smaller δ . And for a certain $a_0 \geq 1$, γ photons with high energy ($\delta \gtrsim \delta_{100}$) obtain increasingly high \bar{h}_γ transferred by the electron spin. For the case of $h_e = 1$, the helicity behavior is similar to that of $h_e = -1$ but slightly different especially at the end of the first few harmonics with $a_0 \lesssim 1$ due to the entanglement term of the laser helicity and electron spin [52]. If electrons are SNP ($h_e = 0$), \bar{h}_γ of γ photons is only provided by the laser helicity. Therefore, \bar{h}_γ of high-energy γ photons via multi-photon absorption channels ($\bar{n} \gtrsim 10$) gradually decreases as a_0 increases, for instance, at $\delta = 0.3$, $\bar{h}_\gamma \approx -0.40$ and -0.03 for $a_0 = 1$ and 10, respectively [see Fig. 2(b)].

Above analytical discussions are based on the single-photon emission of electrons with $\varepsilon_e = 10$ GeV in a monochromatic plane-wave field. However, the transfer mechanism also holds true for other electron energies. The slight difference lies in the positions of harmonic edges and average number of absorbed laser photons [52]. For linearly polarized (LP) γ photons generated in the LP laser, the competition between the laser and

electron for controlling the γ -photon polarization also exists [52]. If electrons are SP, one can increase the laser intensity to generate high-brilliance high-polarization γ rays. However, for SNP electrons, due to the energy regions $\delta \lesssim \delta_1 \propto \varepsilon_e$ for a certain a_0 , apart from the high-intensity laser, higher-energy electrons are also required to produce the similar high-quality γ rays, where the polarization is mainly contributed by the laser via the single-photon absorption channel. Importantly, when scattering process satisfies the rotational symmetry around the collision axis, e.g., in the case of CP laser, the angular momentum conservation holds and one could expect the generation of vortex γ photons with intrinsic orbital angular momentum (OAM) via multi-photon absorption channels. In the monochromatic CP laser, γ photons corresponding to the n -th harmonic carry OAM $l_\gamma = nh_L + h_e - h'_e - h_\gamma$ with the final electron helicity h'_e . Since the radiation dynamics of the vortex γ photons are the same as those of the plane-wave γ photons [50], the transfer mechanism of SAM discussed above is still valid. However, the electrons are required to possess coherence in the transverse plane with axial symmetry in order to attain vortex γ photons.

The manipulation mechanism paves a clear path for high-brilliance high-polarization γ -ray sources. And the generation of CP γ rays via different CS mechanisms in realistic laser pulse is detailed in Fig. 3. The focused Gaussian left-hand CP laser pulse ($h_L = 1$) is employed with peak intensity $a_{0,peak} = 1$, wavelength $\lambda_0 = 0.8 \mu\text{m}$, pulse duration $\tau = 10 T_0$ with the period T_0 , and focal radius $w_0 = 5 \mu\text{m}$. For the head-on colliding cylindrical electron beam, the initial kinetic energy $\bar{\varepsilon}_e = 10$ GeV, energy spread $\Delta\bar{\varepsilon}_e/\bar{\varepsilon}_e = 6\%$, radius $r_e = 2 \mu\text{m}$ with transversely Gaussian profile, longitudinal length $l_e = 3 \mu\text{m}$, polar angle $\theta_e = 180^\circ$ with angular divergence $\Delta\theta_e = 0.2$ mrad, and the electron number $N_e = 5 \times 10^6$. Such electron bunches can be obtained via laser wakefield acceleration [55–58]. In the laser pulse, the intensity sensed by electrons changes in real-time and is strongest at about $T = 35 T_0$ where copious γ rays are radiated [see Fig. 3(a)]. For SNP electrons, the helicities of γ photons come from the laser. In the front of the laser pulse with $T \lesssim 23 T_0$ and $a_0 \lesssim 0.1$, electrons only radiate a small amount of high polarized γ photons due to the low radiation probability of LCS regime [see Figs. 3(a) and 3(b)]. And the polarization directions of γ photons with $\varepsilon_\gamma \gtrsim 1$ GeV ($\delta \gtrsim 0.1$) and $\varepsilon_\gamma < 1$ GeV ($\delta < 0.1$) are opposite [see Figs. 2(b) and 3(b)]. For $23 T_0 \lesssim T \lesssim 35 T_0$, a_0 gradually increases to 1 and since $\delta_1 \propto 1/a_0^2$ the energy regions of $\bar{h}_\gamma \simeq -h_L = -1$ decrease from $\varepsilon_\gamma \lesssim 2$ GeV to $\lesssim 1$ GeV. And there are high-energy γ photons radiated by electrons absorbing dozens of laser photons and \bar{h}_γ of GeV γ photons decreases from ~ -1 to ~ -0.43 due to the decline of the transfer efficiency of laser helicity. As T continues to increase, a_0 begins to decrease and the trends of radiated spectra and helicities of γ photons are basically symmetrical with those of $T \lesssim 35 T_0$. Therefore, the final \bar{h}_γ of γ photons is the comprehensive result due to the laser pulse effect, and the clearly first few harmonics are smoothed out and \bar{h}_γ of γ photons with $\varepsilon_\gamma \gtrsim 2$ GeV is about -0.53 which is higher than $\bar{h}_\gamma \approx -0.43$ of the plane wave with $a_0 = 1$ [see Fig. 2(b) and the green-solid line in Fig. 3(h)]. For LSP elec-

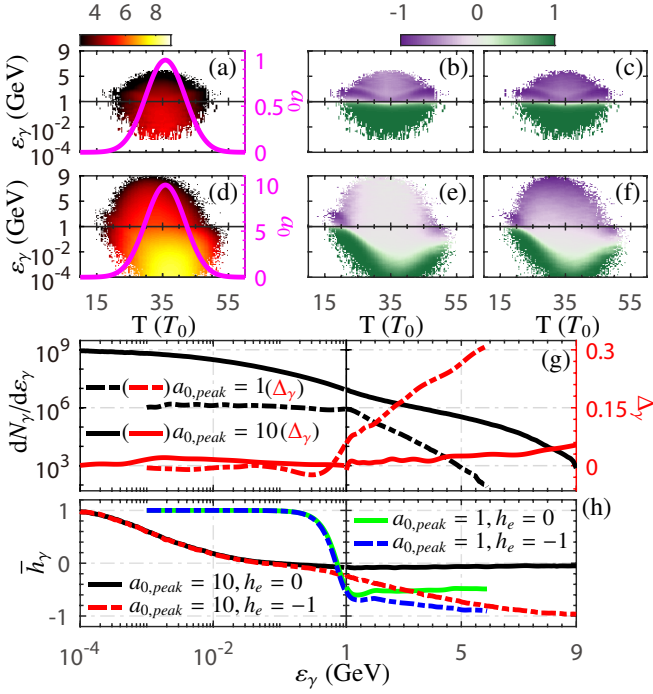


FIG 3. (a)-(c) Generation of γ photons in the realistic laser pulse with peak intensity $a_{0,peak} = 1$ versus the interaction time T (T_0) and γ -photons energy ε_γ with distributions of (a) and (b) the yields $\log_{10} \frac{dN_\gamma}{dT d\varepsilon_\gamma}$ and average helicity \bar{h}_γ for $h_e = 0$, and (c) \bar{h}_γ for $h_e = -1$, respectively, where T_0 is the laser period. The magenta solid line in (a) indicates the laser invariant intensity a_0 in real-time versus T (T_0). (d)-(f) The physical representations and other laser and electron-beam parameters are the same as those in (a)-(c) respectively, except $a_{0,peak} = 10$. Comparisons of (g) energy spectra $dN_\gamma/d\varepsilon_\gamma$ with relative deviation Δ_γ and (h) \bar{h}_γ between the cases of $a_{0,peak} = 1$ and $a_{0,peak} = 10$ versus ε_γ , respectively, where $\Delta_\gamma = (\mathcal{N}^{h_e=-1} - \mathcal{N}^{h_e=0})/\mathcal{N}^{h_e=0}$ and $\mathcal{N} = dN_\gamma/d\varepsilon_\gamma$. Other laser and electron-beam parameters are given in the text.

trons [59–61], the helicities of γ photons contributed by the CP laser are almost identical to the case of SNP electrons for all energy regions radiated at the both ends of the laser pulse with $T \lesssim 23 T_0$ and $T \gtrsim 49 T_0$ and $\varepsilon_\gamma \lesssim 1$ GeV radiated at the middle of the laser pulse with $23 T_0 \lesssim T \lesssim 49 T_0$. However, at the middle of the laser pulse the γ photons with $\varepsilon_\gamma \gtrsim 1$ GeV receive helicities from the scattering electrons and \bar{h}_γ linearly falls (rises) as ε_γ increases for $h_e = -1$ ($h_e = 1$) [see Fig.3(c), the blue-dash-dotted line in Fig.3(h), and [52]]. The relative deviation of energy spectra Δ_γ can reach to 30% (-30%) for $h_e = -1$ ($h_e = 1$) [see the red dash-dotted line in Fig.3(g)].

Usually, one can increase the laser intensity to obtain high-brilliance γ rays. For instance, the γ -photon yields in CS with $a_{0,peak} = 10$ are two to three orders of magnitude higher than those of the $a_{0,peak} = 1$ case [see Figs.3(d) and 3(g)]. And the yield and helicity distributions are not completely symmetric due to the radiation reaction. Importantly, SNP electrons can also generate high-brilliance high-polarization γ rays with the energy scale of keV to MeV [see Fig.3(e) and the black-solid

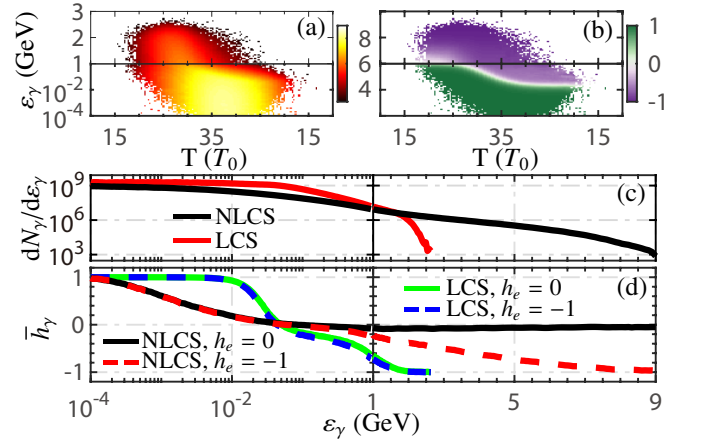


FIG 4. Distributions of γ photons predicted by LCS for SNP electrons ($h_e = 0$) with (a) the yields $\log_{10} \frac{dN_\gamma}{dT d\varepsilon_\gamma}$ and (b) average helicity \bar{h}_γ , respectively. (c) and (d) Comparisons of energy spectra $dN_\gamma/d\varepsilon_\gamma$ and \bar{h}_γ predicted by LCS and NLCS, respectively. The laser and electron-beam parameters are the same as those in Figs.3(d)-3(f).

line in Fig.3(h)]. Similar to the $a_{0,peak} = 1$ case, one gets $|\bar{h}_\gamma| \approx h_L = 1$ for γ photons via linear and weakly nonlinear CS at the front and rear of the laser pulse. During $23 T_0 \lesssim T \lesssim 49 T_0$, the scattering sequentially undergoes weakly nonlinear, strongly nonlinear, and again weakly nonlinear processes. At about $35 T_0$, due to $\delta_1 \propto 1/a_0^2$ the energy regions of $\bar{h}_\gamma \approx h_L = 1$ drop below 100 keV, which is much smaller than that in the plane wave case ($\varepsilon_\gamma = \delta\varepsilon_e \lesssim 10$ MeV) in Fig. 2, due to radiation reaction. Meanwhile, electrons experience the strongest field and have larger probabilities of absorbing thousands of laser photons to radiate higher-energy γ photons; see Fig.3(g). For $\varepsilon_\gamma \gtrsim 1$ GeV, \bar{h}_γ decreases from -0.28 at $T \approx 23 T_0$ to -0.05 at $T \approx 35 T_0$ since the transfer efficiency of laser helicity decreases as a_0 increases. The corresponding brilliances \mathcal{B} (average helicities \bar{h}_γ) are 1.49×10^{20} (0.98), 1.14×10^{21} (0.59) and 5.23×10^{21} (0.16) photons/(s · mm² · mrad² · 0.1%BW) for $\varepsilon_\gamma = 100$ keV, 1 MeV, and 10 MeV, respectively. For LSP electrons, the γ photons spectra are almost identical to the case of $h_e = 0$ with $\Delta_\gamma \approx 5\%$ at $\varepsilon_\gamma = 9$ GeV [see the red-solid line in Fig.3(g)]. However, electrons transfer SAM to high-energy γ photons with $\varepsilon_\gamma \gtrsim 1$ GeV via strongly NLCS and \bar{h}_γ is linearly falling (rising) as ε_γ in the case of $h_e = -1$ ($h_e = 1$) and reaches ≈ -1 (1) at $\varepsilon_\gamma = 9$ GeV [see Fig.3(f), the red-dash-dotted line in Fig.3(h), and [52]]. Note that with $a_{0,peak} = 10$, the locally constant field approximation method commonly used to simulate strongly NLCS performs poorly not only in radiation spectra but also in photon polarization [52, 62–71].

The different helicity behaviors of γ rays in linear and nonlinear CS regimes also represent a clear signal for testing the nonlinear effects of CS (see Fig.4). In LCS, the first cutoff $\delta_1 = \Lambda/(1 + \Lambda) \approx 4\varepsilon_e \varepsilon_L / (m_e^2 + 4\varepsilon_e \varepsilon_L)$ and higher harmonics ($n > 1$) disappear. Therefore, there is a distinct edge at $\varepsilon_{\gamma,edge} = \delta_1 \varepsilon_e = 1.9$ GeV, which is smaller than 2.5 GeV of the

numerical result due to the initial electron energy spread [see the red-solid line in Fig.4(c)]. Furthermore, the helicities of emitted photons are almost completely derived from the laser, and due to the opposite scattering direction, \bar{h}_γ at both ends of the spectra are anti-parallel. And because of the radiation reaction, $\varepsilon_{\gamma,edge}$ and the turning points from $\bar{h}_\gamma \approx 1$ to -1 decrease as T increases [see Figs.4(a) and 4(b)]. As a result, for $10 \text{ MeV} \lesssim \varepsilon_\gamma \lesssim 1 \text{ GeV}$, \bar{h}_γ is averaged to a smaller polarization degree [see the green-solid line in Fig.4(d)]. Therefore, the strongly nonlinear effects not only broaden the spectra but also change the helicity distributions of radiated γ photons compared with the LCS process [see Figs.4(c) and 4(d)]. More significantly, if electrons are LSP, the nonlinear signals will be more sensitive. For instance, the electron spin hardly affects the γ -photon helicity in the LCS process, while, in strongly NLCS, LSP electrons will absorb abundant laser photons and transfer SAM to high-energy γ photons [see Fig.4(d)].

In conclusion, we have investigated the transfer mechanism

of SAM in CS from linear, through weakly into strongly nonlinear regimes to achieve the simultaneous manipulation of high-brilliance and high-polarization of γ rays, paving a way for high-quality polarized γ -beam sources. Moreover, detecting SAM of particles can help us to observe the nonlinear effects of strong field QED processes with currently feasible laser facilities.

Acknowledgment: The work is supported by the National Natural Science Foundation of China (Grants No. 12022506, No. U2267204, No. U2241281), the Foundation of Science and Technology on Plasma Physics Laboratory (No. JCKYS2021212008), the Shaanxi Fundamental Science Research Project for Mathematics and Physics (Grant No. 22JSY014), and Open Foundation of Key Laboratory of High Power Laser and Physics, Chinese Academy of Sciences (SGKF202101).

-
- [1] A. Simon, Theory of Polarized Particles and Gamma Rays in Nuclear Reactions, *Phys. Rev.* **92**, 1050 (1953).
- [2] L. W. Fagg and S. S. Hanna, Polarization Measurements on Nuclear Gamma Rays, *Rev. Mod. Phys.* **31**, 711 (1959).
- [3] F. Zernike, How I Discovered Phase Contrast, *Science* **121**, 345 (1955).
- [4] A. Rousse, C. Rischel, and J.-C. Gauthier, Femtosecond x-ray crystallography, *Rev. Mod. Phys.* **73**, 17 (2001).
- [5] A. Dean, D. Clark, J. Stephen, V. McBride, L. Bassani, A. Bazano, A. Bird, A. Hill, S. Shaw, and P. Ubertini, Polarized gamma-ray emission from the Crab, *Science* **321**, 1183 (2008).
- [6] H. Schworer, J. Magill, and B. Beleites, *Lasers and nuclei: Applications of ultrahigh intensity lasers in nuclear science*, Vol. 694 (Springer Science & Business Media, 2006).
- [7] H. R. Weller, M. W. Ahmed, H. Gao, W. Tornow, Y. K. Wu, M. Gai, and R. Miskimen, Research opportunities at the upgraded HI γ S facility, *Prog. Part. Nucl. Phys.* **62**, 257 (2009).
- [8] D. Budker, J. C. Berengut, V. V. Flambaum, M. Gorchtein, J. Jin, F. Karbstein, M. W. Krasny, Y. A. Litvinov, A. Pálffy, V. Paschalutsa, *et al.*, Expanding nuclear physics horizons with the Gamma Factory, *Ann. Phys.-Berlin* **534**, 2100284 (2022).
- [9] A. Zilges, D. Balabanski, J. Isaak, and N. Pietralla, Photonuclear reactions—From basic research to applications, *Prog. Part. Nucl. Phys.* **122**, 103903 (2022).
- [10] G. Breit and J. A. Wheeler, Collision of Two Light Quanta, *Phys. Rev.* **46**, 1087 (1934).
- [11] Q. Zhao, L. Tang, F. Wan, B.-C. Liu, R.-Y. Liu, R.-Z. Yang, J.-Q. Yu, X.-G. Ren, Z.-F. Xu, Y.-T. Zhao, Y.-S. Huang, and J.-X. Li, Signatures of linear Breit-Wheeler pair production in polarized $\gamma\gamma$ collisions, *Phys. Rev. D* **105**, L071902 (2022).
- [12] Q. Zhao, Y.-X. Wu, M. Ababekri, Z.-P. Li, L. Tang, and J.-X. Li, Angle-dependent pair production in the polarized two-photon Breit-Wheeler process, *Phys. Rev. D* **107**, 096013 (2023).
- [13] O. Halpern, Scattering Processes Produced by Electrons in Negative Energy States, *Phys. Rev.* **44**, 855 (1933).
- [14] D. Micieli, I. Drebot, A. Bacci, E. Milotti, V. Petrillo, M. R. Conti, A. R. Rossi, E. Tassi, and L. Serafini, Compton sources for the observation of elastic photon-photon scattering events, *Phys. Rev. Accel. Beams* **19**, 093401 (2016).
- [15] T. N. Wistisen and U. I. Uggerhøj, Vacuum birefringence by Compton backscattering through a strong field, *Phys. Rev. D* **88**, 053009 (2013).
- [16] S. Bragin, S. Meuren, C. H. Keitel, and A. Di Piazza, High-Energy Vacuum Birefringence and Dichroism in an Ultrastrong Laser Field, *Phys. Rev. Lett.* **119**, 250403 (2017).
- [17] F. Wan, T. Sun, B.-F. Shen, C. Lv, Q. Zhao, M. Ababekri, Y.-T. Zhao, K. Z. Hatsagortsyan, C. H. Keitel, and J.-X. Li, Enhanced signature of vacuum birefringence in a plasma wakefield (2022), arXiv:2206.10792 [physics.plasm-ph].
- [18] D. H. Bilderback, P. Elleaume, and E. Weckert, Review of third and next generation synchrotron light sources, *J. Phys. B: At. Mol. Opt. Phys.* **38**, S773 (2005).
- [19] R. Schwengner, R. Beyer, F. Döna, E. Grosse, A. Hartmann, A. Junghans, S. Mallion, G. Rusev, K. Schilling, W. Schulze, and A. Wagner, The photon-scattering facility at the superconducting electron accelerator ELBE, *Nucl. Instrum. Meth. A* **555**, 211 (2005).
- [20] K. Sonnabend, D. Savran, J. Beller, M. Büssing, A. Constantinescu, M. Elvers, J. Endres, M. Fritzsche, J. Glorius, J. Hasper, J. Isaak, B. Löher, S. Müller, N. Pietralla, C. Romig, A. Sauerwein, L. Schnorrenberger, C. Wälzlein, A. Zilges, and M. Zweidinger, The Darmstadt High-Intensity Photon Setup (DHIPS) at the S-DALINAC, *Nucl. Instrum. Meth. A* **640**, 6 (2011).
- [21] K. Kawase, Y. Arimoto, M. Fujiwara, S. Okajima, M. Shoji, S. Suzuki, K. Tamura, T. Yorita, and H. Ohkuma, MeV γ -ray generation from backward Compton scattering at SPring-8, *Nucl. Instrum. Meth. A* **592**, 154 (2008).
- [22] S. Amano, K. Horikawa, K. Ishihara, S. Miyamoto, T. Hayakawa, T. Shizuma, and T. Mochizuki, Several-MeV γ -ray generation at NewSUBARU by laser Compton backscattering, *Nucl. Instrum. Meth. A* **602**, 337 (2009).
- [23] C. A. Ur, Gamma beam system at ELI-NP, in *AIP Conference Proceedings*, Vol. 1645 (American Institute of Physics, 2015) pp. 237–245.
- [24] M. Bech, O. Bunk, C. David, R. Ruth, J. Rifkin, R. Loewen, R. Feidenhans'l, and F. Pfeiffer, Hard X-ray phase-contrast imaging with the Compact Light Source based on inverse Compton X-rays, *J. Synchrotron Radiat.* **16**, 43 (2009).

- [25] J. Als-Nielsen and D. McMorrow, *Elements of modern X-ray physics* (John Wiley & Sons, 2011).
- [26] F. Albert, S. G. Anderson, D. J. Gibson, C. A. Hagmann, M. S. Johnson, M. Messerly, V. Semenov, M. Y. Shverdin, B. Rusnak, A. M. Tremaine, F. V. Hartemann, C. W. Siders, D. P. McNabb, and C. P. J. Barty, Characterization and applications of a tunable, laser-based, MeV-class Compton-scattering γ -ray source, *Phys. Rev. ST Accel. Beams* **13**, 070704 (2010).
- [27] G. Sarri, D. J. Corvan, W. Schumaker, J. M. Cole, A. Di Piazza, H. Ahmed, C. Harvey, C. H. Keitel, K. Krushelnick, S. P. D. Mangles, Z. Najmudin, D. Symes, A. G. R. Thomas, M. Yeung, Z. Zhao, and M. Zepf, Ultrahigh Brilliance Multi-MeV γ -Ray Beams from Nonlinear Relativistic Thomson Scattering, *Phys. Rev. Lett.* **113**, 224801 (2014).
- [28] S. Gales, K. A. Tanaka, D. L. Balabanski, F. Negoita, D. Stutman, O. Tesileanu, C. A. Ur, D. Ursescu, I. Andrei, S. Ataman, M. O. Cernaianu, L. D'Alessi, I. Dancus, B. Diaconescu, N. Djourelou, D. Filipescu, P. Ghenuche, D. G. Ghita, C. Matei, K. Seto, M. Zeng, and N. V. Zamfir, The extreme light infrastructure—nuclear physics (ELI-NP) facility: new horizons in physics with 10 PW ultra-intense lasers and 20 MeV brilliant gamma beams, *Rep. Prog. in Phys.* **81**, 094301 (2018).
- [29] C. N. Danson, C. Haefner, J. Bromage, T. Butcher, J.-C. F. Chanteloup, E. A. Chowdhury, A. Galvanauskas, L. A. Gizzi, J. Hein, D. I. Hillier, and et al., Petawatt and exawatt class lasers worldwide, *High Power Laser Sci.* **7**, e54 (2019).
- [30] J. W. Yoon, C. Jeon, J. Shin, S. K. Lee, H. W. Lee, I. W. Choi, H. T. Kim, J. H. Sung, and C. H. Nam, Achieving the laser intensity of 5.5×10^{22} W/cm² with a wavefront-corrected multi-PW laser, *Opt. Express* **27**, 20412 (2019).
- [31] J. W. Yoon, Y. G. Kim, I. W. Choi, J. H. Sung, H. W. Lee, S. K. Lee, and C. H. Nam, Realization of laser intensity over 10^{23} W/cm², *Optica* **8**, 630 (2021).
- [32] K. Khrennikov, J. Wenz, A. Buck, J. Xu, M. Heigoldt, L. Veisz, and S. Karsch, Tunable All-Optical Quasimonochromatic Thomson X-ray Source in the Nonlinear Regime, *Phys. Rev. Lett.* **114**, 195003 (2015).
- [33] W. Yan, C. Fruhling, G. Golovin, D. Haden, J. Luo, P. Zhang, B. Zhao, J. Zhang, C. Liu, M. Chen, S. Chen, S. Banerjee, and D. Umstadter, High-order multiphoton Thomson scattering, *Nat. Photonics* **11**, 514 (2017).
- [34] C. Bula, K. T. McDonald, E. J. Prebys, C. Bamber, S. Boege, T. Kotseroglou, A. C. Melissinos, D. D. Meyerhofer, W. Ragg, D. L. Burke, R. C. Field, G. Horton-Smith, A. C. Odian, J. E. Spencer, D. Walz, S. C. Berridge, W. M. Bugg, K. Shmakov, and A. W. Weidemann, Observation of Nonlinear Effects in Compton Scattering, *Phys. Rev. Lett.* **76**, 3116 (1996).
- [35] D. Y. Ivanov, G. Kotkin, and V. Serbo, Complete description of polarization effects in emission of a photon by an electron in the field of a strong laser wave, *Eur. Phys. J. C* **36**, 127 (2004).
- [36] Y. I. Salamin, S. Hu, K. Z. Hatsagortsyan, and C. H. Keitel, Relativistic high-power laser-matter interactions, *Phys. Rep.* **427**, 41 (2006).
- [37] H. Xiao, C.-W. Zhang, H.-B. Sang, and B. S. Xie, Nonlinear Thomson scattering in an arbitrary polarized laser field with a background magnetic field, *Phys. Plasmas* **30**, 10.1063/5.0147858 (2023), 053104.
- [38] T. N. Wistisen and A. Di Piazza, Numerical approach to the semiclassical method of radiation emission for arbitrary electron spin and photon polarization, *Phys. Rev. D* **100**, 116001 (2019).
- [39] B. King and S. Tang, Nonlinear Compton scattering of polarized photons in plane-wave backgrounds, *Phys. Rev. A* **102**, 022809 (2020).
- [40] S. Tang, B. King, and H. Hu, Highly polarised gamma photons from electron-laser collisions, *Phys. Lett. B* **809**, 135701 (2020).
- [41] Y. Wang, M. Ababekri, F. Wan, Q. Zhao, C. Lv, X.-G. Ren, Z.-F. Xu, Y.-T. Zhao, and J.-X. Li, Brilliant circularly polarized γ -ray sources via single-shot laser plasma interaction, *Opt. Lett.* **47**, 3355 (2022).
- [42] Y.-F. Li, R. Shaisultanov, Y.-Y. Chen, F. Wan, K. Z. Hatsagortsyan, C. H. Keitel, and J.-X. Li, Polarized Ultrashort Brilliant Multi-Gev γ Rays via Single-Shot Laser-Electron Interaction, *Phys. Rev. Lett.* **124**, 014801 (2020).
- [43] H. Abramowicz, U. Acosta, M. Altarelli, R. Assmann, Z. Bai, T. Behnke, Y. Benhammou, T. Blackburn, S. Boogert, O. Borysov, et al., Conceptual design report for the LUXE experiment, *Eur. Phys. J. Spec. Top.* **230**, 2445 (2021).
- [44] S. Meuren, Probing strong-field QED at facet-II (SLAC E-320), in *Third conference on extremely high intensity laser physics (ExHILP)*, Vol. 7 (2019).
- [45] B. L. Garrec, S. Sebban, D. Margarone, M. Precek, S. Weber, O. Klimo, G. Korn, and B. Rus, ELI-beamlines: extreme light infrastructure science and technology with ultra-intense lasers, in *High Energy/Average Power Lasers and Intense Beam Applications VII*, Vol. 8962, edited by S. J. Davis, M. C. Heaven, and J. T. Schriempf, International Society for Optics and Photonics (SPIE, 2014) p. 89620I.
- [46] J. P. Zou, C. L. Blanc, D. N. Papadopoulos, G. Chériaux, P. M. Georges, G. Mennerat, F. Druon, L. Lecherbourg, A. Pellegrina, P. Ramirez, F. Giambruno, A. Fréneaux, F. Leconte, D. Badarau, J. M. Boudenne, D. Fournet, T. Valloton, J.-L. Paillard, J. Veray, M. I. Piña, P. Monot, J. P. Chambaret, P. S. Martin, F. Mathieu, P. Audebert, and F. Amiranoff, Design and current progress of the Apollon 10 PW project, *High Power Laser Sci.* **3**, 10.1017/hpl.2014.41 (2014).
- [47] Z. Gan, L. Yu, C. Wang, Y. Liu, Y. Xu, W. Li, S. Li, L. Yu, X. Wang, X. Liu, et al., The Shanghai superintense ultrafast laser facility (SULF) project, in *Progress in Ultrafast Intense Laser Science XVI*, edited by K. M. Kaoru Yamanouchi and L. Roso (Springer International Publishing, Cham, 2021) pp. 199–217.
- [48] A. Gonoskov, T. G. Blackburn, M. Marklund, and S. S. Bulanov, Charged particle motion and radiation in strong electromagnetic fields, *Rev. Mod. Phys.* **94**, 045001 (2022).
- [49] A. Fedotov, A. Ilderton, F. Karbstein, B. King, D. Seipt, H. Taya, and G. Torgrimsson, Advances in QED with intense background fields, *Phys. Rep.* **1010**, 1 (2023).
- [50] M. Ababekri, R.-T. Guo, F. Wan, B. Qiao, Z. Li, C. Lv, B. Zhang, W. Zhou, Y. Gu, and J.-X. Li, Vortex γ photon generation via spin-to-orbital angular momentum transfer in nonlinear Compton scattering, arXiv:2211.05467 [hep-ph].
- [51] K. Yokoya, CAIN 2.42 User Manual (2011).
- [52] See Supplemental Materials for more details on the evolution of γ photon helicity in laser pulse, impact of electron energy (spin) on the transfer mechanism of SAM (average helicity \bar{h}_γ), manipulation of γ ray linear polarization, and comparison of \bar{h}_γ between the methods of locally monochromatic approximation (LMA) and locally constant field approximation (LCFA).
- [53] D. Y. Ivanov, G. Kotkin, and V. Serbo, Complete description of polarization effects in e^+e^- pair production by a photon in the field of a strong laser wave, *Eur. Phys. J. C* **40**, 27 (2005).
- [54] D. Babusci, G. Giordano, and G. Matone, Photon polarization properties in laser backscattering, *Phys. Lett. B* **355**, 1 (1995).
- [55] W. P. Leemans, A. J. Gonsalves, H.-S. Mao, K. Nakamura, C. Benedetti, C. B. Schroeder, C. Tóth, J. Daniels, D. E. Mittelberger, S. S. Bulanov, J.-L. Vay, C. G. R. Geddes, and E. Esarey, Multi-Gev Electron Beams from Capillary-Discharge-Guided

- Subpetawatt Laser Pulses in the Self-Trapping Regime, *Phys. Rev. Lett.* **113**, 245002 (2014).
- [56] G. Xia, Y. Nie, O. Mete, K. Hanahoe, M. Dover, M. Wigram, J. Wright, J. Zhang, J. Smith, T. Pacey, Y. Li, Y. Wei, and C. Welsch, Plasma wakefield acceleration at CLARA facility in Daresbury Laboratory, *Nucl. Instrum. Meth. A* **829**, 43 (2016), 2nd European Advanced Accelerator Concepts Workshop - EAAC 2015.
- [57] A. J. Gonsalves, K. Nakamura, J. Daniels, C. Benedetti, C. Pieronek, T. C. H. de Raadt, S. Steinke, J. H. Bin, S. S. Bulanov, J. van Tilborg, C. G. R. Geddes, C. B. Schroeder, C. Tóth, E. Esarey, K. Swanson, L. Fan-Chiang, G. Bagdasarov, N. Bobrova, V. Gasilov, G. Korn, P. Sasorov, and W. P. Leemans, Petawatt Laser Guiding and Electron Beam Acceleration to 8 GeV in a Laser-Heated Capillary Discharge Waveguide, *Phys. Rev. Lett.* **122**, 084801 (2019).
- [58] F. Li, T. N. Dalichaouch, J. R. Pierce, X. Xu, F. S. Tsung, W. Lu, C. Joshi, and W. B. Mori, Ultrabright Electron Bunch Injection in a Plasma Wakefield Driven by a Superluminal Flying Focus Electron Beam, *Phys. Rev. Lett.* **128**, 174803 (2022).
- [59] M. Wen, M. Tamburini, and C. H. Keitel, Polarized Laser-WakeField-Accelerated Kiloampere Electron Beams, *Phys. Rev. Lett.* **122**, 214801 (2019).
- [60] Z. Nie, F. Li, F. Morales, S. Patchkovskii, O. Smirnova, W. An, N. Nambu, D. Matteo, K. A. Marsh, F. Tsung, W. B. Mori, and C. Joshi, In *Situ* Generation of High-Energy Spin-Polarized Electrons in a Beam-Driven Plasma Wakefield Accelerator, *Phys. Rev. Lett.* **126**, 054801 (2021).
- [61] T. Sun, Q. Zhao, F. Wan, Y. I. Salamin, and J.-X. Li, Generation of ultrabright polarized attosecond electron bunch via dual-wake injection (2022), arXiv:2212.13404 [physics.plasm-ph].
- [62] V. Ritus, Quantum effects of the interaction of elementary particles with an intense electromagnetic field, *J. Sov. Laser Res.* **6**, 10.1007/BF01120220 (1985).
- [63] V. Baier, V. Katkov, and V. Strakhovenko, Quantum radiation theory in inhomogeneous external fields, *Nucl. Phys. B* **328**, 387 (1989).
- [64] C. N. Harvey, A. Ilderton, and B. King, Testing numerical implementations of strong-field electrodynamics, *Phys. Rev. A* **91**, 013822 (2015).
- [65] V. Dinu, C. Harvey, A. Ilderton, M. Marklund, and G. Torgrimsson, Quantum Radiation Reaction: From Interference to Incoherence, *Phys. Rev. Lett.* **116**, 044801 (2016).
- [66] A. Di Piazza, M. Tamburini, S. Meuren, and C. H. Keitel, Implementing nonlinear Compton scattering beyond the local-constant-field approximation, *Phys. Rev. A* **98**, 012134 (2018).
- [67] A. Di Piazza, M. Tamburini, S. Meuren, and C. H. Keitel, Improved local-constant-field approximation for strong-field QED codes, *Phys. Rev. A* **99**, 022125 (2019).
- [68] A. Ilderton, B. King, and D. Seipt, Extended locally constant field approximation for nonlinear Compton scattering, *Phys. Rev. A* **99**, 042121 (2019).
- [69] A. Ilderton, B. King, and A. J. MacLeod, Absorption cross section in an intense plane wave background, *Phys. Rev. D* **100**, 076002 (2019).
- [70] T. Heinzl, B. King, and A. J. MacLeod, Locally monochromatic approximation to QED in intense laser fields, *Phys. Rev. A* **102**, 063110 (2020).
- [71] T. G. Blackburn, A. J. Macleod, and B. King, From local to non-local: higher fidelity simulations of photon emission in intense laser pulses, *New J. Phys.* **23**, 085008 (2021).